MTOpen

# A Collagen-based Scaffold Delivering Exogenous MicroRNA-29B to Modulate Extracellular Matrix Remodeling

Michael Monaghan[1–3], Shane Browne[1], Katja Schenke-Layland[2–4] and Abhay Pandit[1]

[1]Network of Excellence for Functional Biomaterials, National University of Ireland, Galway, Ireland; [2]Department of Cell and Tissue Engineering, Fraunhofer Institute for Interfacial Engineering and Biotechnology, Stuttgart, Germany; [3]University Women's Hospital, Eberhard Karls University, Tübingen, Germany; [4]Department of Medicine/Cardiology, Cardiovascular Research Laboratories, University of California, Los Angeles, CA, USA

Directing appropriate extracellular matrix remodeling is a key aim of regenerative medicine strategies. Thus, antifibrotic interfering RNA (RNAi) therapy with exogenous microRNA (miR)-29B was proposed as a method to modulate extracellular matrix remodeling following cutaneous injury. It was hypothesized that delivery of miR-29B from a collagen scaffold will efficiently modulate the extracellular matrix remodeling response and reduce maladaptive remodeling such as aggressive deposition of collagen type I after injury. The release of RNA from the scaffold was assessed and its ability to silence collagen type I and collagen type III expression was evaluated *in vitro*. When primary fibroblasts were cultured with scaffolds doped with miR-29B, reduced levels of collagen type I and collagen type III mRNA expression were observed for up to 2 weeks of culture. When the scaffolds were applied to full thickness wounds *in vivo*, reduced wound contraction, improved collagen type III/I ratios and a significantly higher matrix metalloproteinase (MMP)-8: tissue inhibitor of metalloproteinase (TIMP)-1 ratio were detected when the scaffolds were functionalized with miR-29B. Furthermore, these effects were significantly influenced by the dose of miR-29B in the collagen scaffold (0.5 versus 5 µg). This study shows a potential of combining exogenous miRs with collagen scaffolds to improve extracellular matrix remodeling following injury.

*Received 13 August 2013; accepted 11 November 2013; advance online publication 25 February 2014. doi:10.1038/mt.2013.288*

## INTRODUCTION

Typically, a complex cascade of events follows cutaneous injury aiming to repair the skin in sequential and overlapping phases beginning with an acute inflammatory response, matrix degradation, and tissue remodeling which subsides to the formation of a mature tissue.[1] Adverse wound healing can lead to excessive scar tissue formation, wound contraction, or nonhealing wounds, which present a major clinical issue in healthcare today. Current approaches at minimizing such adverse wound healing include topical administration of anti-inflammatory agents, inhibitors of gene transcription, inhibitors of growth factors, physical occlusion, and advanced surgical techniques.[2] Biomaterial scaffolds have garnered much attention as mediators of scar formation as they enable increased hydration of the epidermis covering the scar and minimize the risk of infection in the healing wound. These biomaterials include extracellular (ECM) matrix derived scaffolds, serving as physical support to promote tissue organization, resist aggressive wound contraction[3] and scar tissue formation.[4] They also have the potential to deliver bioactive substances such as cytokines,[5] growth factors,[4] living cells,[6] and vectors of gene therapy.

The current tenet of regenerative medicine encompasses the use of biomolecules such as growth factors, pharmaceutical agents, or mediators of genetic engineering. Genetic engineering has progressed to include inhibitors of gene expression, namely, interfering RNA (RNAi).[7] RNAi delivery from a biomaterial enables a localized therapy as the scaffold can act as a reservoir of RNAi, thereby enhancing delivery.[7] Additionally, delivery from a topical scaffold has the potential to maintain effective levels of payload and nucleotide bioactivity for extended periods which increases the likelihood of transfection. The rate of delivery from such a scaffold can be dictated by a combination of the interaction of the therapeutic payload (in the case of this study; RNAi) with the matrix and release during degradation of the scaffold.

MicroRNA (miR)-29B has been specifically correlated with the regulation of fibrosis in a number of tissues including renal,[8] bone,[9] pulmonary,[10] hepatic,[11] and cardiac.[12] miR-29B has been demonstrated repeatedly to be associated with TGF-$\beta_1$ directed fibrogenesis and widely reported to directly target ECM genes such as fibronectin, collagen type I, and collagen type III.[8,10,11] Additionally, miR-29B has been observed to be reduced in expression or completely lost in fibrotic diseases, hence, miR-29B is believed to have a potential antifibrotic role.[12]

After being transcribed and processed from the nucleus, an miR duplex becomes loaded into a RNA induced silencing complex and activated to bind to mRNA and repress gene transcription.[7] The target mRNA is not purely specific as the seed sequence of a mature miR encompasses the first 2–7 or 2–2 nucleotides from its 5′ end and imperfect matches in the 3′ end of the miR

*Correspondence:* Abhay Pandit, Network of Excellence for Functional Biomaterials, National University of Ireland Galway, Galway, Ireland. E-mail: abhay.pandit@nuigalway.ie

strand can be tolerated.[7] As a result, a single miR can regulate multiple cellular targets and, conversely, each gene can be controlled by many miRs. Additionally, miRs can have indirect targets through the silencing of transcriptional factors[13] and dysregulation of molecular pathways. This alone implies an elaborate and multifaceted mechanism of gene regulation, which has yet to be fully elucidated.

Even so, exogenous miRs are being delivered as potential therapeutics in many forms such as pre-miRs transcribed from plasmid DNA or viral vectors, or in their mature form as miR duplexes; such as were employed in this study.

In this study; the *in vitro* and *in vivo* evaluation of a collagen-based scaffold crosslinked with four-arm poly (ethylene glycol) terminated succinimidyl glutarate (4S-StarPEG) doped with miR-29B mature duplexes was performed. The effect of this scaffold on wound healing processes, specifically its impact on ECM remodeling following injury, was evaluated *in vivo*. It is hypothesized that this scaffold, when functionalized with miR-29B and applied to a rat excisional wound model, will modulate the wound healing response by reducing collagen type I production (which is a protein directly silenced by miR-29B) and subsequently ameliorate the collagen type III/I ratio in the remodeling dermis. It is also proposed that miR-29B in combination with the scaffold will work synergistically towards an improvement in wound healing which can be dictated by the dose of miR-29B present in the scaffold.

## DISCUSSION

### *In vitro* development and characterization of miR-29B functionalized collagen scaffold

ECM derived biomaterials as delivery platforms of nonviral therapeutics have been previously documented both *in vitro* and *in vivo*, with beneficial outcomes.[14,15] Previously, the *in vitro* effects of 4S-StarPEG crosslinked collagen type I scaffolds have been investigated as a delivery platform for delivering mesenchymal stem cells.[6] With the four-arm structure of 4S-StarPEG, theoretically, one expects one mole of 4S-StarPEG to react with four moles of free amines available in collagen type I (essentially a 1:4 molar ratio; **Supplementary Figure S1**). With this assumption in mind, the range of crosslinking densities was based around this theoretical optimal value. Determining the effectiveness of crosslinking via TNBSA quantification of free amine groups indicated a decrease in free amine groups that was inversely proportional to an increase in 4S-StarPEG concentration (**Figure 1a**). The percentage of free amines available could be reduced to 9.5% with a 1 mmol/l crosslinking density. Although there was no significant difference between the most effective crosslinking concentrations (1 and 2 mmol/l), there is a trend towards more free amines at 2 mmol/l (17.6%). This is understandable as a saturation of 4S-StarPEG crosslinker can cause steric hindrance to other 4S-StarPEG molecules, thereby incurring less efficient crosslinking. This is supported by the effect of crosslinker on resistance to enzymatic degradation (**Figure 1b**). Resistance to enzymatic degradation was increased in all scaffolds crosslinked with 4S-StarPEG with a significantly higher mass (85%) remaining when crosslinked at a concentration of 1 mmol/l.

Additionally, the 4S-StarPEG concentration had a significant effect on the release of siRNA embedded within the sample (**Figure 1c**). This is due to both an interaction of the siRNA with the 4S-StarPEG and the crosslinker-dependent degradation profile of the collagen scaffold. As RNA has amine, groups present in its backbone it is possible that the crosslinker interacts with these free amines. Such an interaction, however, would be minimal as Cy3 labeling of the RNA occurs via interaction of the Cy3 dye with the free amines available in the RNA. Additionally, the crosslinker is added to the collagen solution first, and then the RNA is added in order to minimize its interaction with 4S-StarPEG. As crosslinker density has an effect on the degradation profile of the scaffold, it is apparent, especially at 0.05 mmol/l crosslinking density, that this degradation plays a key role in the release profile of the RNA. At 2 days, the Cy3 labeled RNA has been completely released, although it should be noted that at this time point and at this concentration, complete degradation of the scaffold had occurred. The 0.5 and 1 mmol/l scaffolds survived the 10-day experiment without complete degradation, and showed a more delayed release of RNA, with 85.45 and 73.88% RNA, respectively, at the final time-point. Further analyses revealed that the nucleic acid, in this case double stranded RNA, cannot interact electrostatically with the 4S-StarPEG crosslinked scaffold and hence is not strongly bound to the scaffold; this is reflected in the electrophoresis data (**Supplementary Figure S3**). Nucleic acid naturally occurs as a negatively charged molecule. The collagen used in this study has been crosslinked using the free amine groups ($NH_2$) present in its backbone, and not the negatively charged carboxyl (COOH) groups, which offers the collagen a net negative charge. Noncrosslinked scaffolds containing RNA present a net positive charge. However, when the scaffolds are crosslinked with 4S-StarPEG, they lose their ability to bind electrostatically with RNA, which accounts for the increased rate of release when embedding naked RNA within the scaffold.

Based on the ability to control the release from this platform, it was sought to achieve a functional effect of this collagen scaffold doped with miR-29B *in vitro*. Delivering naked miR-29B to monolayer cultures did not affect silencing of collagen type I and collagen type III (**Supplementary Figure S2**); however, when embedded within the scaffold, naked miR had a significant silencing effect (**Figure 2**). A profound silencing of collagen type I mRNA occurred (0.66, 0.59, and 0.59 at days 3, 7, and 14, respectively, yet this was only statistically significant at 7 days). miR silencing routinely effects maximum silencing to a degree of 50% which makes these results particularly interesting Collagen type III silencing was not as pronounced up to 14 days in all groups investigated (**Figure 2**) and a recovery in collagen type III mRNA was observed. Collagen has proved to be an effective reservoir of pDNA and siRNA in the past and therefore the observations obtained in this study are consistent with those reported previously.[16,17] Embedding siRNA within a collagen scaffold offers greater protection from RNAses and limits its degradation. Furthermore, cells interact favorably with collagen and this can enable enhanced uptake of a therapeutic nucleic acid.

### Modulation of ECM deposition and wound healing *in vivo*

Full thickness excisional dermal wounds were created on the dorsum of female Lewis rats and the collagen scaffold (crosslinked

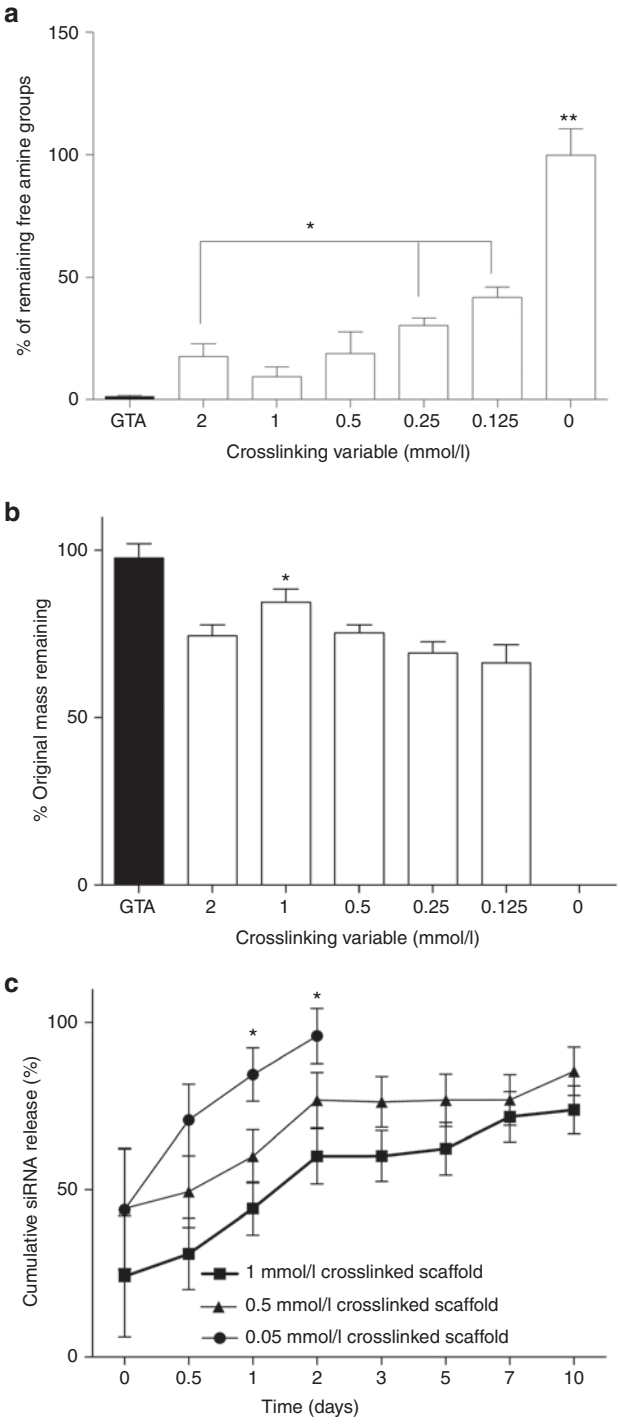


**Figure 1 Quantitative physico-chemical characteristics of RNA releasing tunable collagen scaffold.** (**a**) Quantification of free amine groups after crosslinking with 4S-StarPEG. * indicates statistical significance between 1 mmol/l crosslinking compared with 0.25 and 0.125 mmol/l crosslinking, ** compared with all other groups as in the case of glutaraldehyde (GTA); percentage of remaining amine groups is statistically decreased when compared with all other groups. There exists an inversely proportional relationship between the concentration of 4S-StarPEG and the percentage of free amines remaining in scaffolds after crosslinking. (**b**) Degradation by collagenase quantified by mass remaining after 48 hours. Noncrosslinked control (0) has degraded after 48 hours and therefore no mass is represented. Glutaraldehyde (GTA) was used as a positive control. * indicates a statistically significant difference using one-way ANOVA compared with all other data sets presented in the graph ($n = 3$; $P < 0.05$). (**c**) Release profiles of Cy3 labeled RNA from scaffolds crosslinked with varying concentrations of 4S-StarPEG. Release of Cy3 labeled RNA was determined spectrophotometrically and extrapolating from standard curves. Data presented is the mean ± SD, $n = 4$. * indicates statistically significant release profiles using a 0.05 mmol/l 4S-StarPEG crosslinker concentration compared with concentrations of 1 and 0.5 mmol/l, $P < 0.05$.

with 1 mmol/l 4S-StarPEG for *in vivo* studies), the scaffold doped with 0.5 μg of miR-29B, or the scaffold doped with 5 μg of miR-29B, were placed on the wounds. The migration of the wound margins to the central axis of the wound was evaluated histologically (wound contraction, **Figure 4**) and in all cases, the use of the collagen scaffold with or without miR-29B had a significantly reduced wound contraction when compared with the no treatment control. Wound contraction in the empty scaffold group was reduced significantly by 10% (**Figure 3a**). Contraction of the wound edges is further reduced to 15% when the scaffold is doped with either a low or a high dose of miR-29B when compared with a no treatment control, and this effect is significant. Cutaneous wounds heal through a combination of epithelial migration from the wound margins and contraction of the wound bed to bring the wound margins closer. As these wound edges, come together, collagen fibrils organize parallel to the epidermis, increasing the mechanical strength of the tissue. Wound contraction and scarring, which occur after large injuries can, however, lead to substantial loss of function and poor aesthetic appearance. Wounded areas that can be restricted due to contracted scars will potentially benefit from scaffolds that resist contraction and therefore tension until healing is complete.[18,19] The reduced contraction in the 5 μg miR-29B scaffold group is corroborated when measuring the volume fraction of granulation tissue, revealing a significant increase in volume fraction of granulation tissue when compared with no treatment (55 versus 30%, **Figure 3b**); an effect that was statistically significant when compared with all other groups. This granulation tissue forms the basis upon which new tissue is formed in the wound and is highly vascularized and metabolically active and forms the mechanical substrate upon which the wound exerts contractile forces.[20] The use of miR-29B reduces this contraction resulting in an increased granulation tissue which demonstrates that the mechanism of contraction has been impaired.

In view of this significant effect of the treatment on wound contraction and granulation volume fraction, polarized light microscopy (**Figure 4**) was employed to obtain simultaneous imaging of collagen type I like fibers and collagen type III like fibers (**Figure 3c**). In comparison to native, unwounded skin (which was tissue taken from a remote part of the dorsum and not subjected to any excisional wounding or exposed to any of the treatment groups), all groups, with the exception of the scaffold doped with 5 μg miR-29B, had a statistically significant reduced collagen type III: collagen type I ratio. Alterations in the ratio of collagen type III: collagen type I are hallmark indicators of injury and aging in the skin, which makes this result particularly significant. A reduced collagen type III: collagen type I ratio suggests a stiffer, predominantly collagen type I granulation tissue whereas a higher collagen type III: collagen type I ratio suggests a more compliant, less stiff granulation tissue—which accords with the previous quantitative analyses of wound contraction and granulation volume fractions.

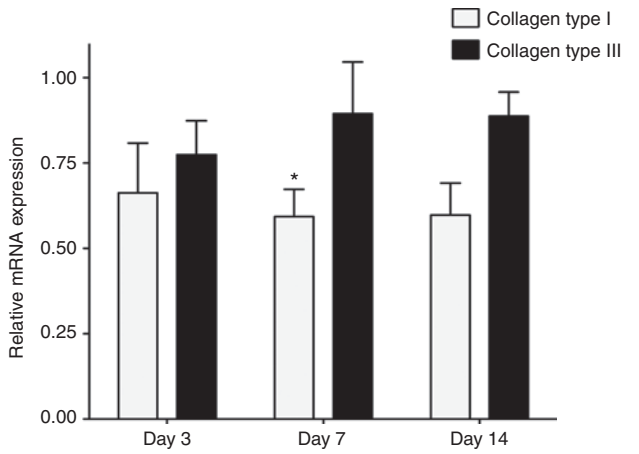


**Figure 2 qRT-PCR data demonstrating the effect of miR-29B in silencing collagen type I and collagen type III mRNA in rat cardiac fibroblasts when delivered from a 1 mmol/l 4S-StarPEG crosslinked collagen scaffold.** Relative mRNA expression was determined by comparing the collagen type I and type III Ct values to the housekeeping GAPDH Ct values, and normalizing with that of rat cardiac fibroblasts treated with a 1 mmol/l 4S-StarPEG collagen scaffold alone (empty control). Asterisk indicates a statistically significant difference compared with the use of a 1 mmol/l 4S-StarPEG crosslinked collagen scaffold alone (all data relative to this group), $P < 0.05$. Data is presented as the mean ± SD, $n = 4$.

This result also suggests, that the miR-29B, at a dose of 5 μg in the scaffold, has a significant effect in restoring the natural balance of collagen type III: collagen type I which otherwise can become deregulated following traumatic injury. Furthermore, immunohistochemical staining of collagen type III expression showed that collagen type III expression was increased in wounds treated with the scaffold and a high dose of miR-29B (**Figure 4**).

To further understand the influence of this platform on wound healing, a biotin label-based rat antibody array, capable of detecting the expression levels of 90 rat proteins was employed. The proteins affected are clustered for clarity; and these include: growth factors such as VEGF, EGFR; apoptotic factors such as Fas Ligand, FADD; ECM remodeling proteins Activin, TGF-βs, tissue inhibitor of metalloproteinase (TIMPs), matrix metalloproteinase (MMPs); and inflammatory cytokines; IL-1α, IL-1β, MCP-1 (**Figure 5**).

The proteins associated with apoptosis, namely *Fas TNFSNF6* and *Fas Ligand TNFSNF6* are downregulated when this scaffold is applied (**Figure 5**). Apoptosis is a morphologically and biochemically distinct process of cell death which is a crucial control mechanism for the development of organs during embryogenesis, and also for the maintenance of tissue homeostasis in mature organisms.[21] It has been identified as a key player in the transition between granulation tissue and the formation of a definitive scar after soft tissue injury[22] as significant apoptosis of fibroblasts, endothelial cells, and pericytes occurs, and appears to affect cell types in successive waves after wound closure. When a wound closes and evolves into a scar, there is a dramatic decrease in cellularity.[23] When applying the platforms developed in this study, complete maturation of granulation tissue and formation of a definitive scar has not evolved based on the evaluation of granulation tissue volume fractions and contraction of the wounds. Indeed, this is in agreement when wound contraction was reduced using a scaffold

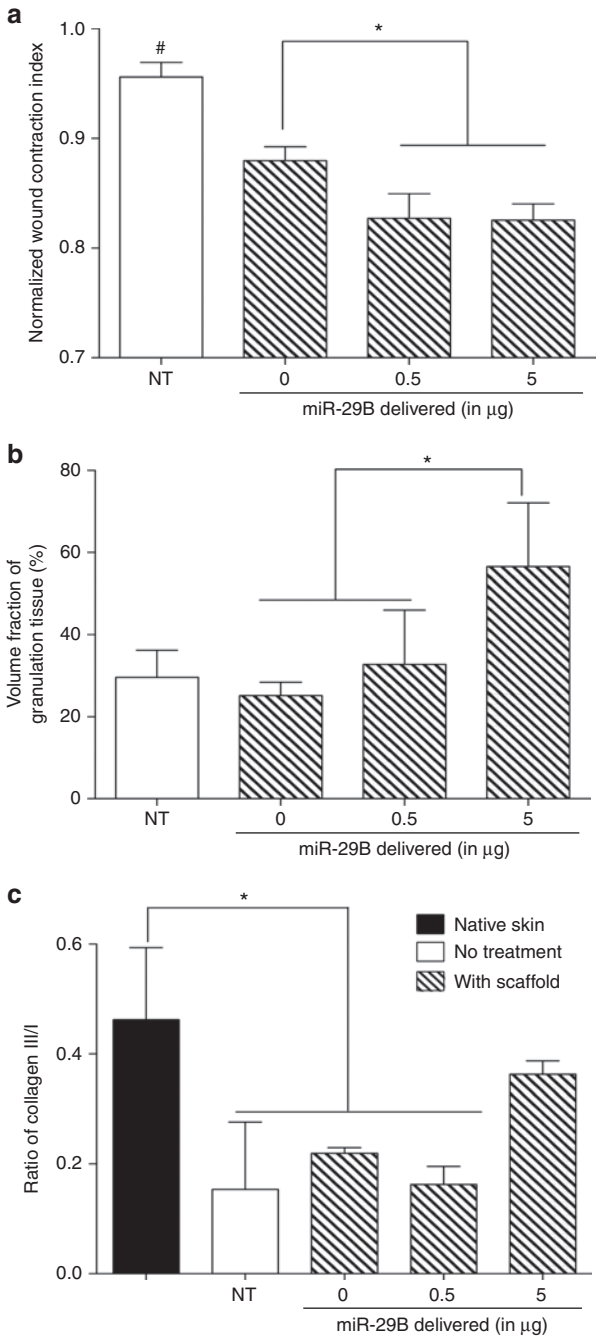


**Figure 3 Quantitative effect of the RNA releasing collagen scaffolds on the healing wound *in vivo*.** (**a**) Effect of treatments on wound contraction (normalized to wound width at day 0). Wound contraction was evaluated with stereological methods using pictures such as the representative images in Figure 4. * indicates statistical significance when compared with indicated groups; $P < 0.05$. # indicates statistical difference compared to all other groups presented $P < 0.05$. (**b**) Normalized wound contraction is the relative decrease in wound margin width at day 28 compared with day 0. Granulation volume fraction was evaluated stereologically using pictures such as the representative images in Figure 4. Granulation volume fraction is indicated by the cyan/blue granulation tissue presented centrally in the images of Figure 4 between the wound margin boundaries and the epithelium. * indicates statistical significance between the groups indicated. (**c**) Ratio of collagen type III-like fibers to collagen type I-like fibers, within the wound bed, determined from sections staining with picrosirius red (representative images in Figure 4). * indicates statistical significance when compared with healthy unwounded skin, $P < 0.05$. Data presented is the mean ± SD analyzed by one-way ANOVA and Tukey's *post hoc* test, $P < 0.05$.

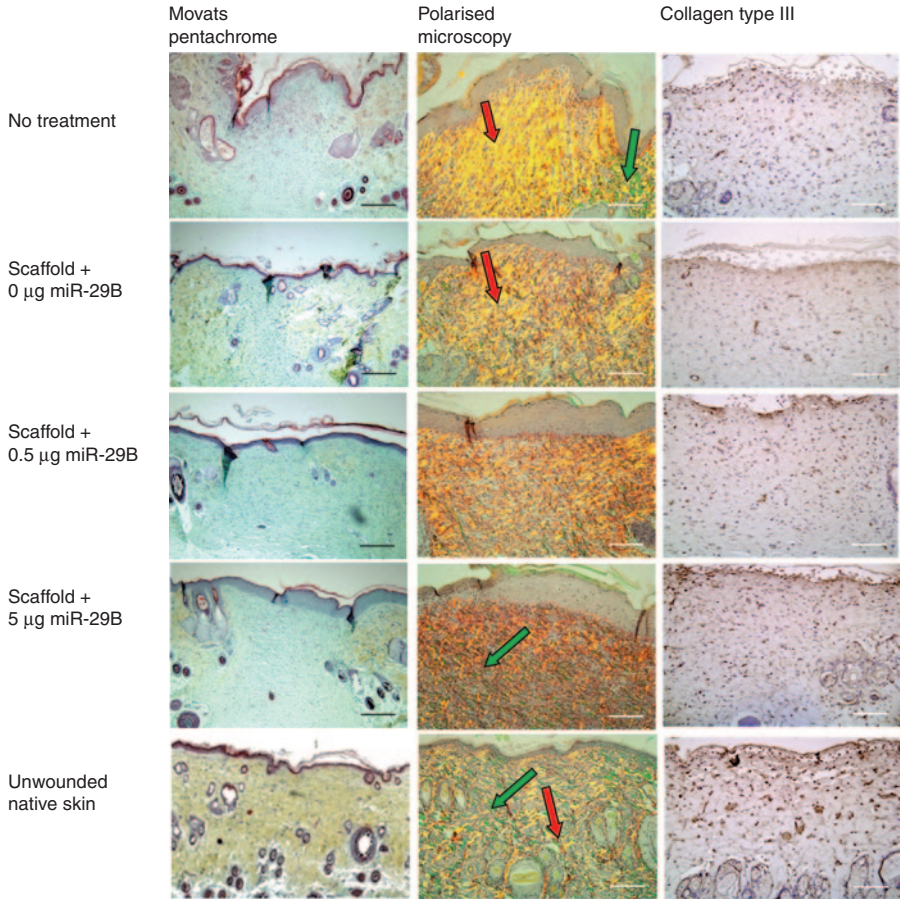


**Figure 4 Representative micrographs of wound beds following treatment with RNA releasing collagen scaffolds.** Representative Russel-Movat's pentachrome staining of wound bed sections at day 28 with blue/cyan representing the field of granulation tissue and yellow being the original skin collagen that indicates the wound margins. Scale bar = 100 µm. Polarized light microscopy of picrosirius red stained wound bed sections. Green-stained fibers demonstrate the presence of collagen type III-like fibers and yellow and red-stained fibers demonstrate the presence of collagen type I-like fibers. Collagen type-I like fibers are highlighted with red arrows within some sections and collagen type-III like fibers are highlighted with green arrows. Sections are counterstained with Weigerts hematoxylin (purple). Scale bar = 100 µm. Micrographs of collagen type III immunohistochemical staining of wound bed sections, counterstained with hematoxylin. Scale bar = 100 µm.

in any case (**Figure 3a**). However, when doping the scaffold at the high dose of 5 µg of miR-29B, apoptotic factors are upregulated. This is extremely significant for a number of reasons. It demonstrates that the miR-29B has an effect on the upregulation of apoptotic proteins and this effect is also dose dependent. The influence of miR-29B on apoptosis has only recently been elucidated. For instance, miR-29B is known to have many targets, one of which is the antiapoptotic protein Mcl-1.[24] Therefore, increased presence of miR-29B can downregulate the transcription of Mcl-1 thereby reducing the inhibition of apoptosis. This accords some agreement with the data obtained from the protein array in which an upregulation of apoptotic proteins is seen when delivering 5 µg of miR-29B in conjunction with a crosslinked scaffold.

The application of a scaffold resulted in a reduction in the expression of inflammatory cytokines. This suggest that the scaffold elicits a minimal host response as it is made of a tellocollagen, a form of collagen without the terminal peptides, eliminating antigenic regions by proteolytic processing.[25] The incorporation of miR-29B into the scaffold elicits an upregulation of some inflammatory cytokines (IL-1α, IL-1β) and this pattern exists for both 0.5 and 5 µg of miR-29B. It is possible that the exogenous miRs are eliciting a mild inflammatory response due to possible activation of toll like receptors[26] or engagement with unidentified genetic targets (directly or indirectly) that promote inflammation.

Based on the observations from the biotin label-based rat antibody array and histological analyses, enzyme-linked immunosorbent assays (ELISAs) were performed to quantify and determine the influence of the treatments on the levels of TIMP-1, MMP-8, and TGF-β1 (**Figure 6a–c**). The observations detected in the membrane protein array with regard to TGF-$\beta_1$, TIMP-1, and MMP-8 expression are, for the most part, in agreement with the ELISAs. Considering the profiles of the key proteins involved in ECM remodeling, TGF-$\beta_1$ is deregulated (in this case, downregulated) when the scaffold is applied (based on protein array data and ELISA quantification). This is accompanied by the downregulation of MMP-2 and MMP-13 (in the membrane protein array), which are known to be stimulated by TGF-$\beta_1$.[27,28] TGF-β is a key mediator of ECM production and has been delivered with biomaterials in order to enhance ECM production. TGF-$\beta_1$ is beneficial in increasing the healing rates of wounds that do not need to be aesthetically appealing; yet the ideal scenario of tissue regeneration requires controlled healing through which there is no exaggerated

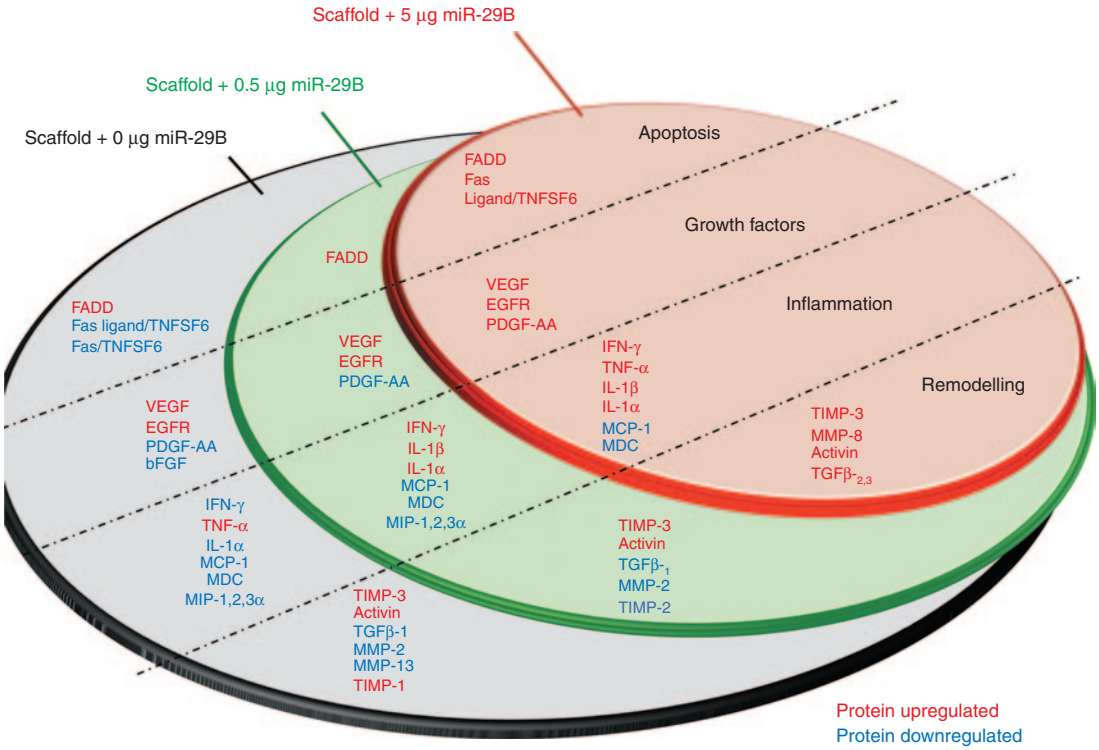


**Figure 5 Venn diagram summarizing the proteins that are upregulated (red) and downregulated (blue).** Proteins are clustered into various pathways such as those indicative of remodeling, growth factors, inflammatory markers and ligands of apoptosis. Proteins that are dysregulated are presented relative to a nontreated excisional wound.

deposition of fibrillar ECM proteins that contribute to unsightly, compromised scar tissue. It is established that miR-29B acts post-transcriptionally on many of the ECM proteins that are stimulated by TGF-$\beta_1$ [12,29]; however, there are many conflicting reports regarding the direct crosstalk between miR-29B and TGF-$\beta_1$.[30,31] TGF-$\beta_1$ has not been established to be a direct target of miR-29B. On the contrary, TGF-$\beta_1$ has been suggested to downregulate endogenous miR-29B expression.[31] Winbanks *et al.*[31] have documented that TGF-$\beta_1$ can attenuate the differentiation of myogenic cells by increasing the expression of histone deacetylase 4, a key inhibitor of myogenic commitment. The underlying mechanism of the increased histone deacetylase 4 was the downregulated expression of miR-29B, which acts as a translational repressor of histone deacetylase 4. A similar pattern has been noted in renal fibrosis where Smad3 mediated TGF-$\beta_1$ has downregulated miR-29B by binding to the promoter of miR-29.[32]

Finally in the context of remodeling; MMPs and their inhibitors, TIMPs, specifically MMP-8 and TIMP-2, play important roles in the degradation and regeneration of wounded tissue.[33] MMPs are inactivated by TIMP-1, TIMP-2, TIMP-3, and TIMP-4 which act by forming a 1:1 complex with the catalytic zinc in the MMPs site.[34] It has been suggested that elevation of TIMP-1 may be a surrogate marker for increased ECM turnover.[35] TIMP-1 is a tissue inhibitor of MMP-8[34] which in turn breaks down collagens type I, II, and III in tissue[36] and MMP-8 is established as a predominant collagenase in healing wounds.[37] The scaffold dosed with 5 μg miR-29B had the lowest level of TIMP-1 expression compared with the other treatments, and this level was statistically significant in comparison with the no treatment control and scaffold with 0.5 μg of miR-29B alone. MMP-8 expression was increased in the wounds treated with a scaffold containing both miR-29B doses in the membrane protein array. Conclusively, the ELISA results show that an empty scaffold had the lowest MMP-8 expression, which was statistically significant when compared with a scaffold with 0.5 or 5 μg of miR-29B in a scaffold.

Appertaining to the levels of MMP-8 and TIMP-1, the ratio of MMP-8 to TIMP-1 (**Figure 6d**) brings further understanding to the results of this study. The use of a scaffold with 5 μg miR-29B resulted in a significantly higher MMP-8: TIMP-1 ratio when compared with all other groups analyzed in this study. This implies that ECM remodeling is on-going as a ratio of 1:1 indicates that the MMP-8: TIMP-1 ratio is balanced but with the application of a scaffold doped with 5 μg miR-29B; this ratio is ~1.4. Although this ratio is not excessively high, it is higher than all the other groups, the greatest of which has a MMP-8: TIMP-1 ratio of 0.5. A linear regression analysis was performed to ascertain if there was a significant trend between the input parameters and the output parameters investigated, and this revealed a statistically significant correlation between the degree of miR-29B doping of the scaffold and the MMP-8: TIMP-1 ratio (**Figure 6d**, Pearson's coefficient $r = 0.9996$; $P = 0.0047$). This analysis reveals that the dose of miR-29B within the scaffold dictates a positive increase in the MMP-8:TIMP-1 ratio based on the dose of miR-29B. Therefore, the employment of a scaffold with miR-29B affects wound healing in which the level of MMP-8 to TIMP-1 is greater, suggesting increased matrix turnover and that this is dependent on the miR-29B dose. This significant ratio is also reflective of the

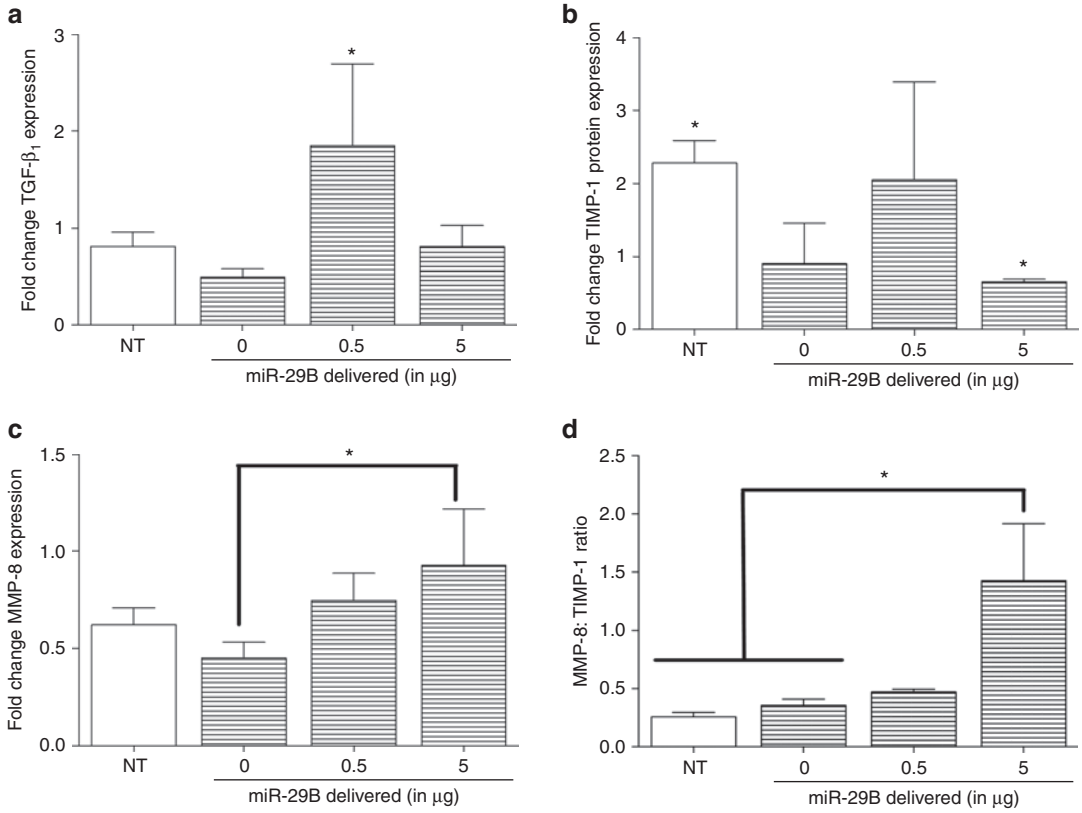


**Figure 6 Quantitation of wound healing factors following treatments with RNA releasing collagen scaffolds *in vivo*.** (**a**) Fold change of TGF-$\beta_1$ expression in excised tissue at day 28, data normalized to healthy unwounded skin. (**b**) Fold change of TIMP-1 expression in excised tissue at day 28, data normalized to healthy unwounded skin. (**c**) Fold change of MMP-8 expression in excised tissue at day 28. (**d**) Ratios of MMP-8 to TIMP-1 expression in excised tissue at day 28, data normalized to healthy unwounded skin. NT indicates an excisional wound with no treatment applied (NT). Data presented is the mean of $n = 4 \pm$ SD analyzed by one-way ANOVA and Tukey's *post hoc* test. * indicates statistical significance between the groups indicated ($P < 0.05$).

collagen type III: collagen type I ratios investigated in **Figure 3c**. The higher MMP-8:TIMP-1 ratio suggests increased matrix turnover and indeed MMP-8 breaks down collagen type I. Therefore, the significance of the findings of both these investigations can be taken as being connected.

A wound healing polymerase chain reaction (PCR) array analysis revealed a number of genes upregulated and downregulated, which were in agreement with results from the protein membrane array and ELISA results (**Supplementary Figures S4 and S5**). Four groups which showed significant results from the membrane protein array and ELISAs were investigated, namely: the scaffold alone, the scaffold with 5 μg miR-29B, the no-treatment control for comparison and healthy skin on which to base the relative expression of the treatments and control upon. B2M, HPRT1, RPL13A, GAPDH were chosen as internal housekeeping controls within each group. For ease of representation, the genes which were upregulated and also downregulated are presented in the form of Venn diagram (**Supplementary Figure S5**); a cut off of a fold change of five was chosen. Gene expression analysis of the scaffold alone versus the scaffold doped with 5 μg miR-29B was conducted to investigate the mechanism underlying improved collagen type III/I ratio when miR-29B is incorporated into the scaffold. Interestingly, this analysis yielded results that contradicted some of the protein expression study results. The most likely explanation for the opposing observations is that, in this study, wound healing gene expression regulation is not occurring only at the mRNA level. Gene expression can be controlled at the posttranscriptional level by modulating the degradation rates of mRNA (as is the function of miRs) and thereby increasing the number of proteins translated per mRNA molecule. It is possible that there are other posttranscriptional controls that are still being unraveled, such as processes that can increase/decrease the affinity between the desired mRNA and ribosomes.[38] It has been observed that protein and mRNA transcript levels do not consistently correlate and that it is not valid to assume that correlation implies causation in this context.[39] Additionally, RT-PCR of tissue explants encompasses the analysis of cells and different sections of the tissue (*i.e.*, dermis and epidermis) which could have discordant expressions of genes and proteins which are more predominant in some cell types. Nevertheless, multiple genes were deregulated when evaluated using PCR Array. Notably, col1a1, col1a2, col3a1, col4a1, and col4a3 were downregulated in the scaffold doped with 5 μg miR-29B compared with the scaffold alone. This is in agreement with numerous reports that document a decrease in ECM gene transcription following delivery or forced overexpression of miR-29B.[9,40] However, TGF-$\beta_1$ gene expression remained unchanged between the samples and unchanged TGF-$\beta_1$ expression would normally correlate with an unchanged col1a1, col1a2, and col1a3 gene expression;

however, in the scaffold doped with 5 μg miR-29B, these genes were downregulated. This is because miR-29B silencing of these genes occurs posttranscriptionally. Notably, the fivefold downregulation of the col1a1, col1a2, and col3a1 gene expression was unique to the scaffold with 5 μg miR-29B.

In conclusion, multiple aspects of the remodeling response were evaluated in this study and from these evaluations there was a significant impact when excisional wounds were treated with the scaffold developed in this study, and when this scaffold was doped with 0.5 or 5 μg miR-29B. Any one of the treatments resulted in a significant reduction in wound closure. Granulation volume fraction was greatest in the wounds treated with scaffolds containing 5 μg of miR-29B. This treatment did not have a significantly lower collagen type III/I ratio when compared with native skin, and also had a statistically significant higher MMP-8: TIMP-1 ratio when compared with all other treatments. The dose of miR-29B in the scaffold had an effect in the majority of the parameters investigated. Notably, there was a significant correlation between the dose of miR-29B when delivered through the scaffold and the MMP-8: TIMP-1 ratio, which indicates that, not only is the combination of these parameters important, but the dose of miR-29B also has a significant effect on the parameters investigated. It can be concluded, that although the scaffold developed in this study alone is beneficial towards reduced wound contraction, incorporation of miR-29B in a dose-dependent manner ameliorates the wound healing process through modulation of MMP-8 and TIMP-1, collagen type I degradation, and the posttranscriptional inhibition of ECM proteins which are being stimulated by TGF-$\beta_1$.

## MATERIALS AND METHODS

***Materials.*** All solvents were of analytical or HPLC grade and were obtained from Sigma-Aldrich Chemical (Arklow, Ireland) unless otherwise stated. All oligonucleotides and primers were purchased from Eurofins MWG GmbH (Ebersberg, Germany). 4S-StarPEG was purchased from JenKem Technology USA (Allen, TX). miR-29B mimic was obtained from Qiagen (Hilden, Germany) with the sequences for rno-miR-29B: 5′-uagcaccauuugaaaucaguguu-3′.

***Atelocollagen/poly (ethylene glycol) ether tetrasuccinimidyl glutarate scaffold preparation.*** Atelocollagen was isolated as described elsewhere.[41] Nine parts of collagen solution (3.5 mg/ml w/v) was gently and thoroughly mixed with one part 10× PBS. The solution was neutralized by the drop-wise addition of 2 mol/l sodium hydroxide (NaOH) until a final pH of 7–7.5 was reached and kept in an ice bath to delay gel formation. 4S-StarPEG was then added at a final concentration of 0.125, 0.25, 0.5, and 1 mm in a volume of 200 μl. 0.625% glutaraldehyde was used as a positive control. The solutions were incubated for 1 hour at 37 °C in a humidified atmosphere to induce gelation.

***TNBSA assay.*** Residual primary amine groups of type I atelocollagen hydrogels were determined using 2,4,6-trinitrobenzenesulfonic acid (TNBSA) detection of amine groups assay as previously described.[42] Briefly, after crosslinking and gel formation, the hydrogels were incubated in 0.1 mol/l sodium bicarbonate pH 8.5. 0.01% of TNBSA was added to the samples and incubated for 2 hours at 37 °C. The reaction was stopped using 10% sodium dodecyl sulphate and 1 mol/l hydrochloric acid (HCl). The samples were then incubated at 120 °C for 15 minutes. Absorbance of each sample was read at 335 nm and the free amine groups quantified by interpolating values from a linear standard curve of known concentrations of glycine.

***Degradation by collagenase.*** Resistance of the hydrogels to enzymatic digestion was evaluated using a collagenase assay. Briefly, hydrogels were incubated for 1 hour in 0.1 mol/l Tris–HCl (pH 7.4), containing 50 mmol/l calcium chloride ($CaCl_2$) at 37 °C. Subsequently, bacterial collagenase type IV (770 units/mg, extracted from *Clostridium histolyticum*), reconstituted in 0.1 mol/l Tris-HCl at a concentration of 10 units/mg collagen type I was added. After incubation for 48 hours at 37 °C, the enzymatic reaction was stopped by the addition of 0.25 mol/l ethylenediaminetetraacetic acid. After vacuum dehydration, the remaining mass was weighed and normalized to the remaining mass of glutaraldehyde crosslinked hydrogels.

***Elution studies.*** The characterization of the 4S-StarPEG collagen type I hydrogel release profile of interfering RNA was performed used siRNA as a model oligonucleotide labeled with Cy3. siRNA was labeled using Silencer siRNA Labelling Kit Cy3 (Ambion; Life Technologies, Carlsbad, CA) according to the manufacturer's instructions. Release of the miRNA complexes was evaluated using the fluorescence from the control siRNA, which was labeled with Cy3. Briefly, the gels were prepared as described above, in a 48-well plate with the additional step of adding 2 μg of Cy3 labeled siRNA. The effect of crosslinking density on the release profiles of siRNA from the scaffolds was investigated using three conditions: a crosslinking density of 1, 0.5, and 0.05 mmol/l. The loaded scaffolds were incubated for 2 hours at room temperature to allow the complexes to associate with the scaffold and for complete gelation to occur. After this time, the gels were individually removed and transferred to the bottom of a 24-well well plate. To this, an equal volume of tris (hydroxymethyl) aminomethane (Tris)-n/ethylenediaminetetraacetic acid buffer (10 mmol/l Tris-HCl and 1 mmol/l ethylenediaminetetraacetic acid, pH = 7.5) was added. At each time point, this process was repeated. At the end of the experiment, the siRNA content of the solutions was quantified by measuring the fluorescence with a Varioskan Flash spectral scanning multimode reader (Thermo Scientific, Vantaa, Finland) and the cumulative release of siRNA complexes from the scaffold was calculated following comparison with a standard curve.

***Scaffold mediated silencing studies.*** Silencing studies were performed on six-well plates seeded with $1 \times 10^6$ cells per well. After 1-day incubation to ensure adherence and acclimatization, scaffolds were placed on the cells. In total, 250 μl of scaffold forming solution was applied to each well. The scaffolds were applied directly to ensure direct contact with cells and also to bring about a direct interaction between the cells and the scaffold. The use of a 250 μl volume applied in a six-well enabled a very thin scaffold to be produced which maintained diffusion of nutrients to ensure viability of the cells.

***RNA extraction.*** RNA extraction was performed on the cells exposed to scaffolds with or without miRNA at 7, 14, and 21 days. One milliliter of TRI Reagent (Applera Ireland, Dublin, Ireland) was added to each construct and incubated for 5 minutes at room temperature. Scaffolds were mechanically disrupted using a sterile pipette tip. Phase separation was performed by adding chloroform (Sigma-Aldrich), and total RNA was purified using an RNeasy kit (Qiagen), according to the supplier's recommended procedure.

***Real-time reverse transcription polymerase chain reaction.*** Total RNA quantity and purity were determined using spectrophotometry at 260 and 280 nm using an ultraviolet spectrophotometer (NanoDrop ND-1000 Spectrophotometer; NanoDrop Technologies, Wilmington, DE,). RNA integrity was checked electrophoretically using the RNA 6000 Nano LabChip kit with an Agilent Bioanalyser 2100 (Agilent Technologies, Cork, Ireland). Reverse transcription (RT) was performed using the ImProm-II RT system according to the manufacturer's protocol (Promega, Southampton, UK). Gene transcription was examined using real-time RT PCR. Reactions were performed and monitored using an ABI 7000 sequence detection system (Applied Biosystems, Foster City, CA) using TaqMan Real-time Gene Expression Mastermix (TaqMan; Applied

Biosystems) and specific primers which are detailed in **Supplementary Table S2**. The primers were designed and their specificity checked using primer-BLAST (www.ncbi.nlm.nih.gov) and their efficiency determined by RT-PCR on tenfold serial dilutions of template cDNA. Gene transcription was inferred from calibration samples and normalized in relation to transcription of the housekeeping gene; glyceraldehydes-3-phosphate dehydrogenase (GAPDH). The $2^{\Delta\Delta\text{-Ct}}$ method was used to calculate relative gene expression for each gene.

*In vivo* rodent skin excisional wound model. All procedures performed were conducted under animal license no. B100/4342 granted by the Irish Department of Health and approved by the Animals Ethics Committee of the National University of Ireland, Galway. In addition, animal care and management followed the Standard Operating Procedures of the animal facility at the National Centre for Biomedical Engineering Science (NCBES). Fourteen Lewis female rats obtained from Harlan Laboratories (Bicester, UK) were allowed to acclimatize to housing conditions for at least seven days prior to use. The animals ranged between 200 and 250 g of body weight. The agents used to anaesthetize the animals were intra-peritoneal xylazine and ketamine (Xylapan and Narketan, Vetoquinol, UK) at a dose rate of 100 and 10 mg/kg, respectively. The objective of this study was to evaluate the effect of the system developed *in vivo* on the maturing phase during wound healing which is characterized by matrix remodeling, terminal and collagen deposition.[43] Therefore, the experimental design included one time period of 28 days, which is an appropriate timepoint at which to evaluate the effect of treatments on ECM remodeling and composition of the maturing wound.[43] The animals were anaesthetized, shaved and the dimensions of the wounds marked with a permanent ink marker. The surgical field was disinfected prior to surgery using iodine. Four full thickness 1 $cm^2$ wounds were then placed at least 1 cm apart on the back of each rat. All procedures were performed under standard general practice principles of asepsis. Antimicrobial therapy and analgesia were administered subcutaneously up to 4 days postsurgery. The positioning of the four treatments was randomized and recorded. The wounds were covered with transparent polyurethane scaffold (Opsite; Smith & Nephew, London, UK). Numbered jackets were used on all the animals with the intention of preventing wound disturbance and facilitating the identification of experimental groups. Extra measures were taken to minimize wound disruption by housing all the animals individually for the duration of the study.

A number of parameters were investigated in this *in vivo* study. The 1 mmol/l 4S-StarPEG collagen scaffold and miR-29B were independently and jointly examined. To investigate the optimal dose delivery regimen through a scaffold, two dosing regimens were employed: a low dose (0.5 μg) and a tenfold higher, high dose (5 μg). The higher dose of 5 μg was chosen as there exist some, albeit few, reports of topical siRNA delivery which range from 1 (ref. [44]) to 8.7 μg.[45] Five micrograms was chosen as a dose reflecting those present in the literature. Furthermore, 0.5 μg was chosen as a low dose as it is a tenfold decrease and is also within the range of siRNA doses employed *in vitro*.[46] Specifically, the groups investigated are detailed in **Table 1**.

***Harvesting and processing of explants.*** Animals were sacrificed by $CO_2$ asphyxiation at the postimplantation time period (28 days). Jackets and scaffolds were carefully removed and the wounds photographed prior to explantation. Samples were divided into one-half and two quarters of tissue. The half section was fixed in 10% neutral buffered formalin for 12 hours maximum to be subsequently embedded in paraffin and sectioned perpendicularly to the wound surface in 3 μm consecutive sections. A modified Movatpentachrome stain[47] was carried out with the Russel–Movat–Pentachrome-stain kit (Mastertechs; Lodi, CA,) to stain ECM components.

**Table 1 Summary of groups investigated in *in vivo* study.**

| Group No. | 1 | 2 | 3 | 4 | 5 |
|---|---|---|---|---|---|
| RNAi dose | No | 0.5 μg | No | 0.5 μg | 5 μg |
| Scaffold | No | No | Yes | Yes | Yes |

***Wound closure.*** Wound closure was determined by comparing the distance between the wound boundaries at the initial time of surgery with the distance between the wound boundaries at day 28. Attempts were made to determine wound closure using tracing paper on the wounds at day 0 and day 28 but no significant difference between any of the groups could be detected using this method. Therefore, wound closure was evaluated using histological data. To account for shrinkage effects due to dehydration and paraffin embedding, wounds were excised at day zero and processed in an identical fashion to those at day 28. Wound closure was calculated using the following formula:

$$\text{Normalized wound contraction} = \frac{W_0 - W_t}{W_0}$$

where $W_0$ is the distance of the wound bed at day 0 and $W_t$ is the distance of the wound bed at day 28.

***Volume fraction of granulation tissue.*** Granulation tissue resulting from the wound healing process was readily distinguished using the Russel–Movat's Pentachrome staining in which granulation tissue stained blue/cyan in contrast to a mature yellow dermis. Micrographs were obtained at a magnification of ×5; in each case the epithelium was horizontal to the image plane. The area of the granulation tissue was determined using ImageJ imaging software (National Institute of Health, Bethesda, MD) and the volume fraction of granulation tissue calculated using the following formula:

$$\text{Volume fraction granulation tissue} = \frac{A_{Gt}}{A_t} \times t$$

Where $A_{Gt}$ is the area of the granulation tissue on the slide, $A_t$ is the area of total tissue present on the slide and $t$ is the thickness.

***Ratio of collagen type III/I.*** Quantitative polarized microscopy was performed on paraffin embedded sections stained with Sirius red dye (Biocolor, Belfast, Northern Ireland), a bifringence enhancer of collagens. The slides were counterstained using Weigerts Hematoxylin for 8 minutes. The Sirius red dye enhancement of bifringence was used to differentiate between collagens types I and III. Collagen type I-like fibers were identified as yellow and red and collagen type III-like fibers in green.[46] In the visualization of the images, a simple polarizing attachment BX-POL (Olympus, South End-on-Sea, UK) was used in a bright field microscope. This device consists of a polarizer (U-POT) inserted in the illumination path and an analyzer (U-ANT) oriented orthogonal to the polarized beam. Images were taken at ×200 magnification in the newly formed tissue within the wound bed and analyzed. This analysis was performed using ImageJ threshold functions and the ratios calculated by dividing the output of collagen type III by collagen type I fiber analysis.

***Collagen type III immunohistochemistry.*** Collagen type III production by the infiltrated fibroblasts in the wound area was elucidated using immunohistochemistry of representative sections. Hydrated sections were subjected to heat-induced antigen retrieval in pH 6.0 citrate buffer in a pressure cooker. The antibody used in the identification was mouse monoclonal to collagen III (Abcam PLC; Cambridge, UK; dilution: 1:50); applied overnight at 4 °C following blocking with goat-block. Endogenous peroxidase was blocked using hydrogen peroxide (DakoCytomation, Ireland) for 5 minutes. An antigoat horse radish peroxidase (HRP) labeled secondary antibody (DakoCytomation, Ireland) was applied for 30

minutes followed by addition of 3,3′ Diaminobenzidine (DAB) chromagen (DakoCytomation, Ireland) and the samples were counterstained with Mayer's Hematoxylin. Three images were taken per slide from six slides per treatment. The location of analysis was medial and the magnification used was ×400. Volume fractions of collagen type III were analyzed using a grid size of 2.5 $\mu m^2$.

***Simultaneous detection of rat protein expression using membrane array.*** Tissue from selected groups was frozen at −80 °C until ready. Tissue was thawed slowly on ice and incubated in a lysis buffer containing a cocktail of protease inhibitors for 5 minutes. The tissue was mechanically disrupted using a bead mill homogenizer (TissueLyserLT; Qiagen) for 5 minutes at least twice until tissue was completely homogenized and centrifuged at 15,000*g* for 15 minutes. The protein fraction of the centrifuged sample was extracted, aliquoted and stored at −80 °C until further use. The protein content of the samples was determined using a protein quantification assay kit (BioRad, Hercules, CA) and probed for 90 proteins simultaneously using a biotin label-based rat antibody array (RayBio; Norcross, GA) according to the manufacturer's instructions. Briefly, four samples were pooled according to the treatment group to a total of 1 mg/ml and dialyzed overnight to remove remaining lysis buffer and the protein membranes were blocked using a provided blocking buffer. The proteins were labeled with biotin using amines present in proteins and incubated with the antibody-labeled membranes overnight. Following this, HRP-conjugated streptavidin was reacted with the membranes and subsequently treated with the incubation buffer provided. Membranes were exposed using a Kodak Image Station 4000MM Pro (Kodak, Japan). Membrane exposures were evaluated using ImageJ software (NIH, Bethesda, MD) plug-ins. The images obtained were imported into ImageJ and analyzed using a protein array analyzer plug-in by normalizing to the given positive control signals on the membranes. For relative comparison, all samples were normalized to healthy native skin, which was not wounded and untreated.

***TGF-$\beta_1$, MMP-8, and TIMP-1 quantification.*** Three ELISAs were performed using protein, which had been aliquoted from the protein isolated for the protein membrane array. The ELISAs included one for transforming growth factor (TGF)-$\beta_1$ (Abcam PLC, Cambridge, UK), MMP-8 (Abcam PLC, Cambridge, UK), and TIMP-1 (R&D Systems, Minneapolis, MN). An equal amount and concentration of each protein sample was added to each well for each ELISA plate which was determined using a protein assay kit (BioRad). ELISAs were performed according to the manufacturer's instructions.

RNA extraction. One milliliter of TriReagent (Applera Ireland, Dublin, Ireland) was added to each tissue sample and incubated for 5 minutes at room temperature. The tissue was mechanically disrupted using a bead mill homogenizer (TissueLyserLT; Qiagen) at least twice for 5 minutes until the tissue was completely homogenized. Phase separation was performed by adding chloroform, and total RNA was purified using an RNeasy kit (Qiagen), according to the supplier's recommended procedure.

***Wound healing RT-PCR array.*** Contaminating DNA was eliminated from RNA preparations using DNase I. The yield and quality of total RNA was determined according to the ratio of spectrophotometric absorbance values at wavelengths of 260 and 280 nm. cDNA synthesis was performed using DNase-treated RNA and random decamer primers using an $RT^2$ First Strand Kit (Qiagen). The cDNA generated was used as a template for quantitative real-time PCR. A mastermix was prepared using a $RT^2$ SYBR Green Mastermix. This mixture was added to 384 wells in an $RT^2$ Profiler PCR Array, Rat Wound Healing Array (PARB-0121Z; Qiagen). The standard cycling conditions were as recommended by the PCR array supplier. Data were collected at the end of the annealing step. Fold changes in gene expression between the affected and control groups were calculated using the $2^{\Delta\Delta}$Ct method in the PCR array data analysis template. An examination of Ct value consistency for the housekeeping genes indicated that normalization was performed adequately. A similar evaluation of the built-in RNA controls verified an absence of genomic DNA contamination and inhibitors of either the reverse transcription or PCR.

***Statistical analysis.*** All samples were tested in triplicate and all experimental groups were analysed in triplicate. GraphPad Prism (v.5 GraphPad Software; San Diego, CA) was used for statistical analysis. Analysis of variance (ANOVA) was used followed by Tukey's *post hoc* test to determine statistical significance between groups. ANOVA was performed assuming normal distribution of the data, which was tested and verified using the Anderson–Darling test. All graphical data is presented as mean ± standard deviation of mean. $P$ values of $< 0.05$ were considered statistically significant. Outliers were calculated using Grubb's test and eliminated from the results to be analyzed. Where appropriate, linear regression analysis was performed where significance was set at $P < 0.05$.

## ACKNOWLEDGMENTS

This work is funded by Science Foundation Ireland under Strategic Research Cluster Grant No. 07/SRC/B1163, Fraunhofer-Gesellschaft (Attract 692263 to K.S.-L.), the Ministry of Science, Research and the Arts of Baden-Württemberg (33-729.55-3/214 to K.S.-L.) and travel support from the European Molecular Biology Organization and the DeutscherAkademischerAustauschDienst. The authors would like to acknowledge Yixao Dong and Yolanda Garcia (National University of Ireland, Galway) for assistance with *in vivo* studies, Oliver Carroll (NFB, National University of Ireland, Galway) for advising on the protein arrays and Shannon Layland (Fraunhofer IGB, Stuttgart, Germany) for editorial assistance.

## SUPPLEMENTARY MATERIAL

**Figure S1**. Type I atelocollagen and 4S-StarPEG reaction. Succinimidyl glutarate is an NHS-ester which binds with amine groups and therefore the succinimidyl groups react with the amine groups present on the molecules of type I atelocollagen at 37 °C.

**Figure S2**. qRT-PCR data demonstrating the effect of miR-29B in silencing collagen type I and type III mRNA in vitro in rat cardiac fibroblasts compared to scrambled control 48 hours after delivery of miR mimics.

**Figure S3**. Agarose gel electrophoresis to indicate the binding of RNA complexes to the collagen 4S-StarPEG scaffold.

**Figure S4**. An example heat map of gene expression data obtained from wound healing RT-PCR array.

**Figure S5**. Overview of number of genes altered in the different comparisons studied in the PCR array analysis with fold change cut off being five.

**Table S1**. Rheological evaluation of crosslinked scaffolds.

**Table S2**. Sequences of primers used in RT-PCR.

## REFERENCES

1. Stadelmann, WK, Digenis, AG and Tobin, GR (1998). Physiology and healing dynamics of chronic cutaneous wounds. *Am J Surg* **176**: 26S–38S.
2. Murphy, PS and Evans, GR (2012). Advances in wound healing: a review of current wound healing products. *Plast Surg Int* **2012**: 190436.
3. Yannas, IV, Burke, JF, Orgill, DP and Skrabut, EM (1982). Wound tissue can utilize a polymeric template to synthesize a functional extension of skin. *Science* **215**: 174–176.
4. Formiga, FR, Pelacho, B, Garbayo, E, Abizanda, G, Gavira, JJ, Simon-Yarza, T *et al.* (2010). Sustained release of VEGF through PLGA microparticles improves vasculogenesis and tissue remodeling in an acute myocardial ischemia-reperfusion model. *J Control Release* **147**: 30–37.
5. Ghahary, A, Tredget, EE, Shen, Q, Kilani, RT, Scott, PG and Takeuchi, M (2000). Liposome associated interferon-alpha-2b functions as an anti-fibrogenic factor in dermal wounds in the guinea pig. *Mol Cell Biochem* **208**: 129–137.
6. Hoban, DB, Newland, B, Moloney, TC, Howard, L, Pandit, A and Dowd, E (2013). The reduction in immunogenicity of neurotrophin overexpressing stem cells after intra-striatal transplantation by encapsulation in an in situ gelling collagen hydrogel. *Biomaterials* **34**: 9420–9429.
7. Monaghan, M and Pandit, A (2011). RNA interference therapy via functionalized scaffolds. *Adv Drug Deliv Rev* **63**: 197–208.
8. Liu, Y, Taylor, NE, Lu, L, Usa, K, Cowley, AW Jr, Ferreri, NR *et al.* (2010). Renal medullary microRNAs in Dahl salt-sensitive rats: miR-29b regulates several collagens and related genes. *Hypertension* **55**: 974–982.

9. Li, Z, Hassan, MQ, Jafferji, M, Aqeilan, RI, Garzon, R, Croce, CM *et al.* (2009). Biological functions of miR-29b contribute to positive regulation of osteoblast differentiation. *J Biol Chem* **284**: 15676–15684.
10. Cushing, L, Kuang, PP, Qian, J, Shao, F, Wu, J, Little, F *et al.* (2011). miR-29 is a major regulator of genes associated with pulmonary fibrosis. *Am J Respir Cell Mol Biol* **45**: 287–294.
11. Roderburg, C, Urban, GW, Bettermann, K, Vucur, M, Zimmermann, H, Schmidt, S *et al.* (2011). Micro-RNA profiling reveals a role for miR-29 in human and murine liver fibrosis. *Hepatology* **53**: 209–218.
12. van Rooij, E, Sutherland, LB, Thatcher, JE, DiMaio, JM, Naseem, RH, Marshall, WS *et al.* (2008). Dysregulation of microRNAs after myocardial infarction reveals a role of miR-29 in cardiac fibrosis. *Proc Natl Acad Sci USA* **105**: 13027–13032.
13. Kim, DH, Saetrom, P, Snøve, O Jr and Rossi, JJ (2008). MicroRNA-directed transcriptional gene silencing in mammalian cells. *Proc Natl Acad Sci USA* **105**: 16230–16235.
14. Viñas-Castells, R, Holladay, C, di Luca, A, Díaz, VM and Pandit, A (2009). Snail1 down-regulation using small interfering RNA complexes delivered through collagen scaffolds. *Bioconjug Chem* **20**: 2262–2269.
15. Holladay, C, Power, K, Sefton, M, O'Brien, T, Gallagher, WM and Pandit, A (2011). Functionalized scaffold-mediated interleukin 10 gene delivery significantly improves survival rates of stem cells in vivo. *Mol Ther* **19**: 969–978.
16. Inaba, S, Nagahara, S, Makita, N, Tarumi, Y, Ishimoto, T, Matsuo, S *et al.* (2012). Atelocollagen-mediated systemic delivery prevents immunostimulatory adverse effects of siRNA in mammals. *Mol Ther* **20**: 356–366.
17. Krebs, MD, Jeon, O and Alsberg, E (2009). Localized and sustained delivery of silencing RNA from macroscopic biopolymer hydrogels. *J Am Chem Soc* **131**: 9204–9206.
18. Kwan, P, Hori, K, Ding, J and Tredget, EE (2009). Scar and contracture: biological principles. *Hand Clin* **25**: 511–528.
19. Zurada, JM, Kriegel, D and Davis, IC (2006). Topical treatments for hypertrophic scars. *J Am Acad Dermatol* **55**: 1024–1031.
20. Hinz, B (2006). Masters and servants of the force: the role of matrix adhesions in myofibroblast force perception and transmission. *Eur J Cell Biol* **85**: 175–181.
21. Kerr, JF, Wyllie, AH and Currie, AR (1972). Apoptosis: a basic biological phenomenon with wide-ranging implications in tissue kinetics. *Br J Cancer* **26**: 239–257.
22. Desmoulière, A, Badid, C, Bochaton-Piallat, ML and Gabbiani, G (1997). Apoptosis during wound healing, fibrocontractive diseases and vascular wall injury. *Int J Biochem Cell Biol* **29**: 19–30.
23. Desmoulière, A, Redard, M, Darby, I and Gabbiani, G (1995). Apoptosis mediates the decrease in cellularity during the transition between granulation tissue and scar. *Am J Pathol* **146**: 56–66.
24. Zhang, YK, Wang, H, Leng, Y, Li, ZL, Yang, YF, Xiao, FJ *et al.* (2011). Overexpression of microRNA-29b induces apoptosis of multiple myeloma cells through down regulating Mcl-1. *Biochem Biophys Res Commun* **414**: 233–239.
25. Ogawa, S, Onodera, J, Honda, R and Fujimoto, I (2011). Influence of systemic administration of atelocollagen on mouse livers: an ideal biomaterial for systemic drug delivery. *J Toxicol Sci* **36**: 751–762.
26. Grelier, A, Cras, A, Balitrand, N, Delmau, C, Lecourt, S, Lepelletier, Y *et al.* (2013). Toll-like receptor 3 regulates cord blood-derived endothelial cell function *in vitro* and in vivo. *Angiogenesis* **16**: 821–836.
27. Kim, ES, Sohn, YW and Moon, A (2007). TGF-beta-induced transcriptional activation of MMP-2 is mediated by activating transcription factor (ATF)2 in human breast epithelial cells. *Cancer Lett* **252**: 147–156.
28. Leivonen, SK, Chantry, A, Hakkinen, L, Han, J and Kahari, VM (2002). Smad3 mediates transforming growth factor-beta-induced collagenase-3 (matrix metalloproteinase-13) expression in human gingival fibroblasts. Evidence for cross-talk between Smad3 and p38 signaling pathways. *J Biol Chem* **277**: 46338–46346.
29. Maurer, B, Stanczyk, J, Jüngel, A, Akhmetshina, A, Trenkmann, M, Brock, M *et al.* (2010). MicroRNA-29, a key regulator of collagen expression in systemic sclerosis. *Arthritis Rheum* **62**: 1733–1743.
30. Luna, C, Li, G, Qiu, J, Epstein, DL and Gonzalez, P (2011). Cross-talk between miR-29 and transforming growth factor-betas in trabecular meshwork cells. *Invest Ophthalmol Vis Sci* **52**: 3567–3572.
31. Winbanks, CE, Wang, B, Beyer, C, Koh, P, White, L, Kantharidis, P *et al.* (2011). TGF-beta regulates miR-206 and miR-29 to control myogenic differentiation through regulation of HDAC4. *J Biol Chem* **286**: 13805–13814.
32. Qin, W, Chung, AC, Huang, XR, Meng, XM, Hui, DS, Yu, CM *et al.* (2011). TGF-ß/Smad3 signaling promotes renal fibrosis by inhibiting miR-29. *J Am Soc Nephrol* **22**: 1462–1474.
33. Nagase, H and Woessner, JF Jr (1999). Matrix metalloproteinases. *J Biol Chem* **274**: 21491–21494.
34. Pradhan-Palikhe, P, Vesterinen, T, Tarkkanen, J, Leivo, I, Sorsa, T, Salo, T *et al.* (2010). Plasma level of tissue inhibitor of matrix metalloproteinase-1 but not that of matrix metalloproteinase-8 predicts survival in head and neck squamous cell cancer. *Oral Oncol* **46**: 514–518.
35. Dinh, W, Füth, R, Scheffold, T, Bansemir, L, Köhler, T, Lapp, H *et al.* (2009). Increased serum levels of tissue inhibitor of metalloproteinase-1 in patients with acute myocardial infarction. *Int Heart J* **50**: 421–431.
36. Brinckerhoff, CE and Matrisian, LM (2002). Matrix metalloproteinases: a tail of a frog that became a prince. *Nat Rev Mol Cell Biol* **3**: 207–214.
37. Muller, M, Trocme, C, Lardy, B, Morel, F, Halimi, S and Benhamou, PY (2008). Matrix metalloproteinases and diabetic foot ulcers: the ratio of MMP-1 to TIMP-1 is a predictor of wound healing. *Diabet Med* **25**: 419–426.
38. Gry, M, Rimini, R, Strömberg, S, Asplund, A, Pontén, F, Uhlén, M *et al.* (2009). Correlations between RNA and protein expression profiles in 23 human cell lines. *BMC Genomics* **10**: 365.
39. Greenbaum, D, Jansen, R and Gerstein, M (2002). Analysis of mRNA expression and protein abundance data: an approach for the comparison of the enrichment of features in the cellular population of proteins and transcripts. *Bioinformatics* **18**: 585–596.
40. Ogawa, T, Iizuka, M, Sekiya, Y, Yoshizato, K, Ikeda, K and Kawada, N (2010). Suppression of type I collagen production by microRNA-29b in cultured human stellate cells. *Biochem Biophys Res Commun* **391**: 316–321.
41. Zeugolis, DI, Paul, RG and Attenburrow, G (2008). Factors influencing the properties of reconstituted collagen fibers prior to self-assembly: animal species and collagen extraction method. *J Biomed Mater Res A* **86**: 892–904.
42. Garcia, Y, Collighan, R, Griffin, M and Pandit, A (2007). Assessment of cell viability in a three-dimensional enzymatically cross-linked collagen scaffold. *J Mater Sci Mater Med* **18**: 1991–2001.
43. Braiman-Wiksman, L, Solomonik, I, Spira, R and Tennenbaum, T (2007). Novel insights into wound healing sequence of events. *Toxicol Pathol* **35**: 767–779.
44. Zheng, D, Giljohann, DA, Chen, DL, Massich, MD, Wang, XQ, Iordanov, H *et al.* (2012). Topical delivery of siRNA-based spherical nucleic acid nanoparticle conjugates for gene regulation. *Proc Natl Acad Sci USA* **109**: 11975–11980.
45. Lee, WR, Shen, SC, Zhuo, RZ, Wang, KC and Fang, JY (2009). Enhancement of topical small interfering RNA delivery and expression by low-fluence erbium:YAG laser pretreatment of skin. *Hum Gene Ther* **20**: 580–588.
46. Cuttle, L, Nataatmadja, M, Fraser, JF, Kempf, M, Kimble, RM and Hayes, MT (2005). Collagen in the scarless fetal skin wound: detection with picrosirius-polarization. *Wound Repair Regen* **13**: 198–204.
47. Russell, HK Jr (1972). A modification of Movat's pentachrome stain. *Arch Pathol* **94**: 187–191.